ELSEVIER

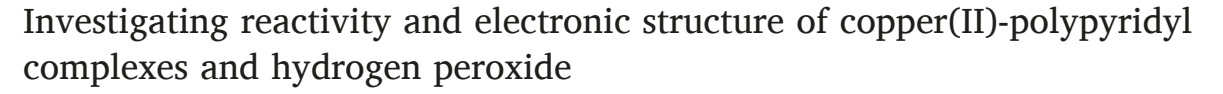
Contents lists available at ScienceDirect

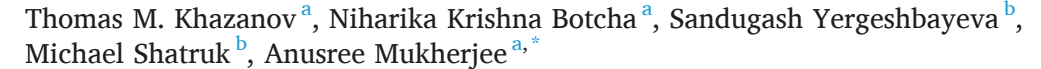
Inorganica Chimica Acta

journal homepage: www.elsevier.com/locate/ica



Research paper





- ^a Department of Chemistry, University of Alabama in Huntsville, 301 Sparkman Drive, Huntsville, AL 35899, United States
- ^b Department of Chemistry and Biochemistry, Florida State University, Tallahassee, FL 32306, United States

ARTICLE INFO

Keywords: Cu-mediated oxidation Enzyme modeling C—H bond activation Epoxidation

ABSTRACT

This work presents a detailed study of the reactivity of three mononuclear Cu^{II} complexes supported by derivatives of the tetradentate ligand N,N'-bis(2-pyridylmethyl)-1,2-ethylenediamine (bispicen). The Cu^{II} complexes are capable of performing C—H bond activation in the presence of NEt₃ and H_2O_2 through what has been proposed computationally to be a $[CuO]^+$ intermediate. A wavefunction-based quantum chemical investigation into the electronic structure of the proposed $[CuO]^+$ intermediate reveals a triplet ground state predominantly consistent with an $S = \frac{1}{2} Cu^{II}$ center ferromagnetically coupled to an oxyl radical, though contributions from the corresponding biradicaloid Cu^I -oxene resonance structure may be nontrivial. Furthermore, correlation of the electronic structure of the proposed intermediate with analogous high-valent metal-oxo species capable of olefin epoxidation suggests that the Cu^{II} complexes might be also capable of olefin epoxidation in the presence of NEt₃ and H_2O_2 . To test this hypothesis experimentally, the Cu^{II} complexes are treated with NEt₃ and H_2O_2 in the presence of alkene substrates, resulting in the formation of epoxides.

1. Introduction

In biology, copper plays a variety of essential roles primarily related to electron transfer [1]. In particular, a number of enzymes that utilize copper as a cofactor are dedicated to O2 binding, activation, and reduction, typically coupling this process with the oxidation of exogenous substrates [2-4]. This oxidation chemistry is accomplished by the generation of reactive copper-oxygen intermediates in mononuclear, binuclear, and even trinuclear and tetranuclear active sites [1,5]. Binuclear sites, in particular, have been implicated in the binding and activation of O2 for substrate oxidation, though the discovery of monooxygenase metalloenzymes containing mononuclear copper active sites such as lytic polysaccharide monooxygenase (LPMO) has resulted in increased interest in monocopper-O₂ species [1,5,6]. The enzyme particulate methane monooxygenase (pMMO), responsible for the oxidation of methane to methanol (bond dissociation energy 104 kcal/mol) [7], has been shown to only contain mononuclear copper sites [8,9]. As the active site was generally believed to be multinuclear until 2019, the mechanism of methane oxidation at a mononuclear copper site remains an open question.

Decades of enzymatic and modelling studies have established that mononuclear copper-oxygen complexes may belong to one of three categories: 1:1 Cu:O₂ complexes, Cu^{II}-alkyl/hydroperoxide complexes, or high valent [CuO]⁺/ [CuOH]²⁺ species [3]. While detailed structural, spectroscopic, and mechanistic understanding has been obtained from the study of systems featuring [CuO₂]⁺ or [CuOOH]⁺/ [CuOOR]⁺ cores, higher valent [CuO]⁺ intermediates have remained particularly elusive as they have only been observed experimentally in the gas phase [1,3]. High valent [CuO]+ species have been proposed as reactive intermediates in enzymes such as dopamine β -monooxygenase, [10,11] peptidylglycine α -hydroxylating monooxygenase [12,13], LPMO [14], as well as in pMMO [15,16]. However, the formulation of high valent [CuO]⁺ species as Cu^{III}-oxo intermediates, in analogy to other high valent metal-oxo species of biological relevance such as Fe^{IV}-oxo [17–20] or Mn^{IV}-oxo [21–23] intermediates, is challenging. Initial theoretical investigations have suggested that [CuO]⁺ systems should be similar or even more powerful oxidants than the analogous and extensively studied Fe^{IV}-oxo complexes [24], and the study of their electronic structure and reactivity seeks to address fundamental questions in both metalloenzymology and inorganic chemistry.

E-mail address: anusree.mukherjee@uah.edu (A. Mukherjee).

^{*} Corresponding author.

Recently we reported experimental and theoretical results that implicated a $[CuO]^+$ species as the reactive intermediate for C—H bond activation [25]. Reactive intermediates were generated from mononuclear Cu^{II} complexes supported by tetradentate polypyridyl ligands with H_2O_2 in an analogous manner to the biological peroxide shunt pathway, bypassing the need for external electrons [26]. In these experiments, substrate oxidation was observed when each copper complex was treated with H_2O_2 and base in the presence of either cyclohexadiene (CHD) or dihydroanthracene (DHA). On the basis of isotope labeling studies, spectroscopic analysis of degradation products, and density functional theory (DFT) calculations, a mechanism for C—H bond oxidation by a $[CuO]^+$ species largely analogous to the radical rebound mechanism of other high-valent metal-oxo species was proposed [27].

Herein we report the reactivity of three mononuclear copper complexes supported by bispicen ligand variants (Fig. 1) toward C—H bond activation. This study further refines our understanding of the electronic structure of the $[\text{CuO}]^+$ species generated from 1 to 3 with H_2O_2 . In addition to C—H bond activation, we use an *ab initio* quantum mechanical investigation into the electronic structure of the proposed $[\text{CuO}]^+$ intermediates and the knowledge of the electronic structure of well-understood epoxidation catalysts to predict complexes 1–3 as being able to perform O-atom transfer to alkenes to form epoxides. As a proof of concept, we further support this claim with reactivity studies of 1–3 toward exogenous alkene substrates.

2. Experimental

2.1. Materials and methods

All reagents and solvents were purchased from MilliporeSigma and Fisher Scientific and directly used for synthesis without further purification unless mentioned otherwise. Copper complexes and ligands were synthesized following reported procedures [28,29]. 9,10-dihydroanthracene (DHA) was purchased from MilliporeSigma and recrystallized from ethanol prior to use. All electronic absorption spectra were measured using an Agilent Cary 8454 UV–Vis Spectrophotometer. Samples for optical spectroscopy were prepared in quartz cells with an optical path length of 1 cm. Graphical representation and data analysis were performed in Origin. Quantification of the oxidized products was carried out using an Agilent 6890 Gas Chromatograph (GC) equipped with an Agilent 5973 Network Mass Selective Detector and Flame Ionization Detector (FID) using naphthalene as an internal standard.

2.2. General procedure for substrate oxidation

Forty equivalents of substrate with respect to the complex were added to solutions of complexes $1{\text -}3$, followed by the addition of ${\rm H_2O_2}$ and ${\rm NEt_3}$ solutions in acetonitrile (10 eq. with respect to the complex) under aerobic conditions at 298 K. Reaction progress was monitored via electronic absorption spectroscopy and products were identified after removal of the copper complex using a microscale alumina column. Product yields were calculated with respect to the copper complexes.

2.3. Computational methods

All computations were carried out using the computational chemistry software package ORCA 4.2 [30]. Geometry optimizations were

Fig. 1. Copper complexes studied in the present work.

carried out with the density functional BP86 [31,32] using the crystal structures of 1 and 2 as a starting point. Calculations employed the def2-TZVP basis set [33,34] for copper and directly coordinated atoms; remaining atoms were calculated using the def2-SV(P) basis set [35]. Dispersion effects were included using the atom-pairwise correction with Becke-Johnson damping scheme (D3BJ) as it has been adopted in the ORCA program [36,37]. The density fitting and "chain of spheres" (RIJCOSX) [38] approximations were employed in conjunction with the auxiliary basis set def2/J [39]. Stationary points were verified by analytic computation of vibrational frequencies. Damping parameters were adjusted as needed in order to reach convergence using the keyword SlowConv. Electron paramagnetic resonance (EPR) parameters were obtained from single-point calculations on the previously optimized geometries using the hybrid density functional B3LYP [40,41]. Scalar relativistic effects were included with the zeroth order regular approximation (ZORA) [42-44] employing the core property basis set CP(PPP) on copper, the ZORA-def2-TZVP(-f) basis set [33,34] on nitrogen and oxygen atoms, and the ZORA-def2-SVP basis set [35] on all remaining atoms. Auxiliary basis sets were generated automatically (AutoAux) [45]. Picture change effects were included. Electronic absorption spectra were calculated for 1-3 within the time-dependent density functional theory (TDDFT) formalism employing the Tamm-Dancoff approximation (TDA) [46] with the same functional and combination of basis sets. Consistent with experiment, solvation effects associated with acetonitrile were accounted for by using the conductor-like polarizable continuum model (CPCM) as implemented in ORCA [30].

The geometries of [1-O]⁺, [2-O]⁺, and [3-O]⁺ were optimized on the broken symmetry (BS) potential energy surface. Single-point calculations were carried out to obtain singlet-triplet gaps and quasi-restricted orbitals (QROs) using the same combination of basis sets described above at the B3LYP, M06 [47], and ωB97X [48] levels of theory. To correct for biradical character in the singlet structures, wavefunctions were calculated employing the complete active space self-consistent field (CASSCF) [49] method. In the CASSCF calculations, an active space consisting of twelve electrons in seven orbitals was chosen (CAS (12,7)). QROs from the single-point calculations of [1-O]⁺, [2-O]⁺, and [3-O]⁺ were used as starting orbitals for the CASSCF calculations. Dynamical correlation effects were explicitly introduced as described by second-order N-electron valence perturbation theory (NEVPT2) to obtain singlet-triplet splittings [50,51]. To better account for dynamical correlation effects, the Cu-4d orbitals were also included, giving rise to a final active space of 12 electrons in 12 orbitals (CAS(12,12)) for the CASSCF/NEVPT2 calculations.

Alternative active spaces and multireference configuration interaction procedures were explored. An active space consisting of fourteen electrons in the five Cu-3d based molecular orbitals (MOs) and three O-2p orbitals was chosen (CAS(14,8)). Orbitals with an occupation less than 1.98 and greater than 0.02 from the CAS(14,8) calculations were used to construct reference spaces of 10 electrons in 6 orbitals (10,6) for subsequent spectroscopy oriented configuration interaction calculations (SORCI) [52]. While (8,5) reference spaces may have been sufficient for [1-O]⁺ and [3-O]⁺, a (10,6) reference space was required to describe the electronic structure of [2-O]⁺ based on orbital occupation, so (10,6) reference spaces were constructed for all three compounds for consistency. All CASSCF and SORCI calculations were carried out with the ZORA-def2-TZVP(-f) basis set on copper, nitrogen, and oxygen atoms and the ZORA-def2-SVP basis set on all other atoms.

2.4. X-ray crystallography

Single-crystal X-ray diffraction was performed on a Rigaku-Oxford Diffraction Synergy-S diffractometer equipped with a HyPix detector and a Mo- $K\alpha$ radiation source ($\lambda=0.71073$ Å). In a typical experiment, a single crystal was suspended in Parabar® oil (Hampton Research) and mounted on a cryoloop that was cooled to the desired temperature in an N₂ cold stream. The data sets were recorded as ω -scans at 0.5° step width

and integrated with the CrysAlis [53] software package. Empirical absorption correction was applied as implemented in the SCALE3 ABSPACK algorithm [54]. The crystal structure solution and refinement were carried out with SHELX [55] using the interface provided by Olex2 [56]. The final refinement was performed with anisotropic atomic displacement parameters for all atoms. Full details of the crystal structure refinement and the final structural parameters have been deposited with the Cambridge Crystallographic Data Centre (CCDC). The CCDC registry numbers and a brief summary of data collection and refinement parameters are given in Table S1.

3. Results and discussion

3.1. Synthesis and characterization

The syntheses of L^{1-3} were performed according to previously published procedures [28,29,57,58]. Copper complexes were similarly synthesized according to published procedures [28,29]. Complexes 1-3 exhibit broad optical absorption bands with maxima in the 588-620 nm range. These bands are assigned to d-d transitions, typical of mononuclear Cu(II) compounds in square pyramidal geometry [28,59-63]. We previously reported the crystal structure of 1 and herein report the structures of 2 obtained under two different conditions [28].

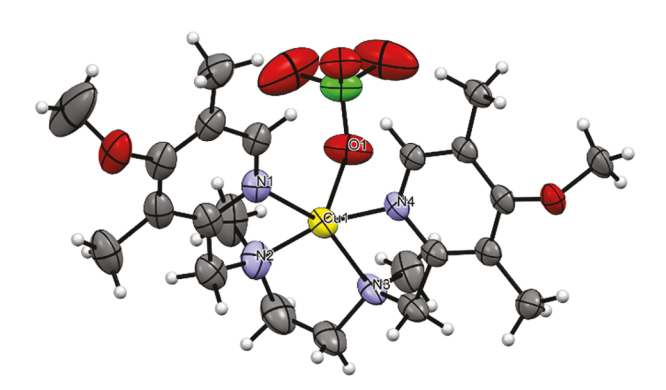
X-ray quality single crystals of 2a were obtained by vapor diffusion of diethyl ether into an acetone solution of the complex at room temperature. The copper center is coordinated in a distorted squarepyramidal geometry ($\tau = 0.16$) with four coordination sites occupied by the nitrogen atoms of the ligand and the fifth axial site occupied by one oxygen atom from the perchlorate counterion (Fig. 2). The Cu-N bond lengths are consistent with known Cu(II) complexes supported by N4 ligands in a distorted square pyramidal geometry. X-ray quality single crystals of 2b were obtained by vapor diffusion of diethyl ether into an acetonitrile solution of the complex at room temperature. When crystals were obtained from an acetonitrile solution, the coordinating perchlorate ion in 2a is replaced by a molecule of coordinating solvent (MeCN). The copper center is similarly coordinated in a distorted square pyramidal geometry ($\tau = 0.26$) in which ligand nitrogen atoms occupy the equatorial coordination sites and the axial site is occupied by coordinating acetonitrile. The distortion from square pyramidal geometry is greater than in 2a but the observed geometry is still consistent with other square pyramidal copper(II) complexes in the literature [28,63].

Axial coordination of solvent when crystals were obtained from acetonitrile attests to the lability of the axial coordination site. This was also observed in the previously reported crystal structure of complex 1 in which water is axially coordinated [28]. For this reason, computational models were constructed with axially coordinated MeCN as consistent with experiment. The calculated bond distances in the DFT-optimized geometries of 2a and 2b are in reasonable agreement with the crystal

structure (Table 1). While the equatorial Cu-N distances are generally slightly overestimated and the axial Cu-N/O bond slightly underestimated in the DFT-optimized structure, the elongation of the axial Cu-N/O relative to the equatorial Cu-N bonds of the ligand is correctly predicted by the computational model. These small discrepancies between experimental and calculated bond lengths may be attributed to crystal packing forces [64]. The computed optical parameters of 1 and 2 (Table S2) were in broad agreement with the experimentally obtained results, slightly overestimating the absorption maximum of 2. The calculated EPR spin Hamiltonian parameters (Tables S3-4) for 1-2 were in similar agreement. The rhombicity of the g-tensor was apparent for 2 at X-band, slightly deviating from axial symmetry as predicted by the computational studies (Table S3). Higher frequencies are required to observe similar deviations for 1 and 3, and all are compared under approximate axial symmetry for consistency. This agreement between the observed and calculated spectroscopic parameters for 1-2 suggests that the computationally derived structure of 3 can be correlated to the experimentally obtained optical and EPR spectra within the same computational methodology. As crystals of 3 suitable for crystallography could not be obtained, this provides some insight into the geometric structure of 3 and allows for comparison with complexes 1-2. The electronic absorption spectrum of 3 is well reproduced by the computed electronic transitions (Table 2), exhibiting one optical band centered at approximately 600 nm assigned to a d-d transition at the metal center [28]. This is consistent with mononuclear Cu^{II} complexes in square pyramidal geometry, as it is known that mononuclear Cu^{II} complexes in a trigonal-bipyramidal geometry typically exhibit absorption maxima at longer wavelengths [65-67]. The calculated electronic g-tensor for **3** is approximately axial $(g_1 > g_2 \gtrsim g_3 > g_e)$, consistent with a square pyramidal or elongated octahedral geometry with the unpaired electron residing mainly in the $3d_{x^2-y^2}$ orbital [63,68,69]. The calculated g-values are slightly underestimated compared to the experimentally obtained values. Taking the ⁶³Cu hyperfine coupling tensor as axial, an increased A_{\parallel} value and reduced A_{\perp} value is obtained relative to experiment. The spectral parameters are generally in agreement, however, and consistent with the proposed structure.

3.2. Reactivity toward H₂O₂

Addition of H_2O_2 (10 eq.) to a solution of 1 in MeCN in the presence of NEt₃ (10 eq.) resulted in an initial redshift of the d-d transition band centered at 588 nm and subsequent decay to a well-defined optical band centered at 641 nm with a shoulder above 400 nm (Fig. 3). In the case of 2, treatment with H_2O_2 in the presence of NEt₃ resulted in rapid decay of the broad d-d transition band centered at 620 nm (Fig. S1). This absorbance band decayed to a new feature centered at 634 nm and lower in intensity than that of the starting material. A more narrow, intense feature was observed for 2 at 492 nm after the decay of the original



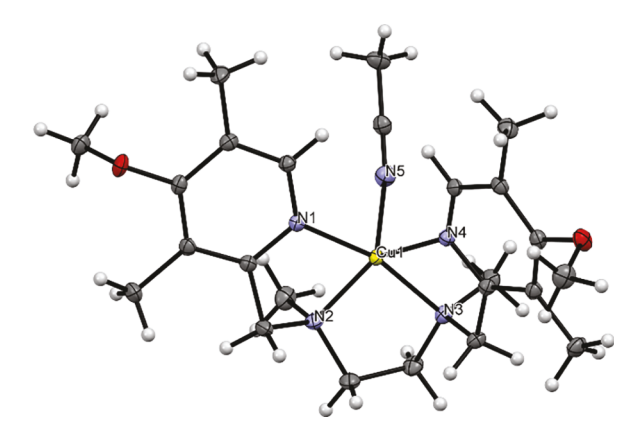


Fig. 2. Left: ORTEP view of complex 2a crystallized from acetone/diethyl ether; right: ORTEP view of complex 2b crystallized from acetonitrile/diethyl ether.

Table 1
Selected bond distances and bond angles for complexes 2a and 2b.

| | Bond Distances (Å) | | | | | Bond Angles (degrees) | | | |
|--------|--------------------|-------|-------|-------|-----------|-----------------------|-------|--------|-------|
| | 2a | | 2b | | | 2a | | 2b | |
| | Exp. | Calc. | Exp. | Calc. | | Exp. | Calc. | Exp. | Calc. |
| Cu1–N1 | 2.007 | 2.018 | 2.012 | 2.012 | N1-Cu1-N2 | 82.60 | 82.0 | 81.77 | 80.9 |
| Cu1-N2 | 2.018 | 2.073 | 2.037 | 2.094 | N2-Cu1-N4 | 165.80 | 164.9 | 149.03 | 139.5 |
| Cu1-N3 | 2.009 | 2.131 | 2.034 | 2.087 | N2-Cu1-N3 | 85.20 | 85.9 | 85.23 | 85.4 |
| Cu1-N4 | 2.002 | 1.994 | 2.027 | 2.030 | N1-Cu1-N3 | 156.10 | 137.8 | 164.66 | 163.3 |
| Cu1-O1 | 2.308 | 2.127 | _ | _ | N1-Cu1-O1 | 103.10 | 127.3 | _ | _ |
| Cu1-N5 | - | - | 2.176 | 2.118 | N1-Cu1-N5 | - | - | 92.17 | 94.8 |

Table 2Optical and magnetic parameters for complex **3**. The g-tensor axes were assumed to be collinear with the Cu hyperfine coupling tensor principal axes. Experimental values obtained from ref. 30.

| | Absorption Maxima (nm) | g values | | Cu hyperfine coupling constants (MHz) | |
|-----------------------------|------------------------|-----------------|----------------------|---------------------------------------------|-----------------|
| | | g_{\parallel} | \mathbf{g}_{\perp} | A_{\parallel} | ${\sf A}_\perp$ |
| Experimental Theoretical | 606 572 | 2.216 2.148 | 2.051 2.047 | 540 587 | 60 37 |

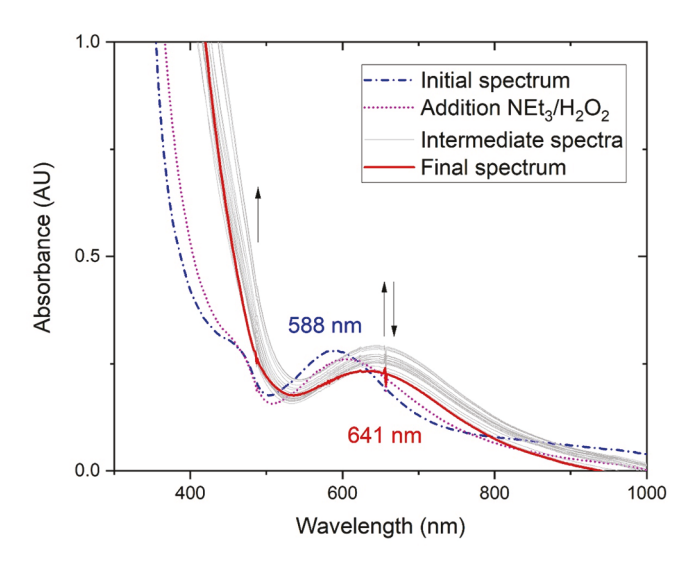


Fig. 3. Reaction of 1 with 10 eq. H_2O_2 and 10 eq. NEt_3 in MeCN monitored for 6 h *via* electronic absorption spectroscopy. Optical path length 1 cm.

optical band at 620 nm and formation of the feature around 634 nm. Treatment of **3** with 10 eq. NEt₃/ H_2O_2 elicited similar spectral changes to those observed for **1** (Fig. S2). As observed with other known copper complexes mimicking peroxide shunt chemistry, the spectral changes observed for **1**–**3** were dependent on the presence of both NEt₃ and H_2O_2 [25,70]. From this we infer the formation of at least one new species in solution upon addition of H_2O_2 and NEt₃.

3.3. C-H bond activation

Having previously observed similar reactivity towards NEt $_3/H_2O_2$ with related complexes [25], we were curious whether these complexes would also be capable of oxidizing exogenous hydrocarbon substrates. The reactivity of **1–3** toward **1,4-cyclohexadiene** (CHD) and **9,10-dihydroanthracene** (DHA) in the presence of NEt $_3/H_2O_2$ was similarly explored spectroscopically. Treatment of **1** with 10 eq. NEt $_3/H_2O_2$ in the presence of 40 eq. of CHD or DHA resulted in final absorption spectra (Fig. 4) that lacked a well-defined optical band due to increased

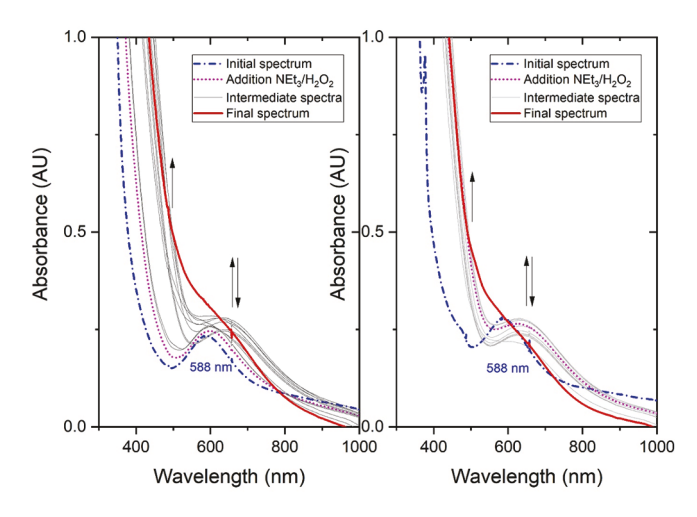


Fig. 4. Left: Reaction of **1** with 10 eq. H_2O_2 , 10 eq. NEt_3 , and 40 eq. CHD in MeCN monitored for 6 h via electronic absorption spectroscopy. Right: reaction of **1** with 10 eq. H_2O_2 , 10 eq. NEt_3 , and 40 eq. DHA in MeCN monitored for 6 h via electronic absorption spectroscopy. Optical path length 1 cm.

absorbance in the 400-500 nm region compared to treatment with only NEt₃ and H₂O₂ (Fig. 3), prompting us to analyze the reaction mixtures for oxidized substrate. Similar increases in absorbance in the 400-500nm region of the final spectra were observed for 2 and 3, as well (Fig. S3-6). Analysis of the product solutions by gas chromatography-mass spectrometry (GC-MS) established the oxidation of both substrates by 1-3. In the case of DHA, anthraquinone, anthracene, and anthrone were identified as products, while benzene was obtained as the major product of CHD oxidation. Similar yields were obtained for all three complexes (Table 4), despite the variations in the ligand architecture. The reactivity of 1-3 toward NEt₃/H₂O₂, CHD, and DHA was consistent with the previously reported reactivity of copper complexes supported by other bispicen-type ligands in which computational studies suggested the feasibility of a [CuO]+ intermediate as the reactive intermediate responsible for CHD and DHA oxidation [25]. This similarity in reactivity led us to further investigate the electronic structure of the [CuO]⁺ species generated from 1 to 3 to better understand their reactivity.

3.4. Electronic structure of [LCuO]⁺

Computation of the electronic structure of [CuO]⁺ species proves somewhat challenging due to its multiconfigurational nature. As a single determinant theory, Kohn-Sham (KS) DFT is not sufficient for the study of systems not well described by a single Slater determinant [71,72]. Multiconfigurational approaches such as the complete active space self-consistent field (CASSCF) method and multireference second-order perturbation theory (CASPT2) have been applied to the problem at hand in a related system to overcome these limitations inherent to KS DFT [24]. Here, we consider an analogous approach in which second-order *N*-electron valence perturbation theory (NEVPT2) is applied to

the CASSCF wavefunction to obtain corrections to the energy.

Dioxygen may be considered as a test case for the CASSCF/NEVPT2 method for which the CASSCF/CASPT2 method has already been applied and experimental data is available [24], allowing for parallels to be drawn between the well-understood electronic structure of diatomic molecules and the [CuO] core of the more complex polyatomic molecules reported here. Diatomic O2 possesses five low-lying states that have been rigorously examined spectroscopically: the ground state ${}^{3}\Sigma_{\sigma}^{-}$, and the four excited states $^1\Delta_g, ^1\Sigma_g^+, ^3\Sigma_u^+,$ and $^3\Sigma_u^-$ [73]. We first examine the transition between the $^3\Sigma_g^-$ and $^1\Delta_g$ states, separated by 0.98 eV (22.6 kcal mol⁻¹) [24,74]. A singlet-triplet gap of 1.00 eV (23.13 kcal mol⁻¹) was predicted by the CASSCF/NEVPT2 method employing a fullvalence active space, reaching the desired chemical accuracy of $\pm\,1$ kcal mol^{-1} [75]. The $^{1}\Delta_{g}$ state is well described by a single configuration. Considering additional excited states, the CASSCF/NEVPT2 method correctly predicts a multiconfigurational state located 1.65 eV (38.00 kcal/mol) above the ground state, consistent with the experimentally observed singlet biradical $^1\Sigma_{\rm g}^+$ state located 1.63 eV (37.51 kcal/mol) above the $^3\Sigma_g^-$ state [76,77]. This is an important test case for the study of the electronic structure of [CuO]⁺ species because the formally Cu^{III}oxo formulation is a closed-shell singlet, as is the ${}^{1}\Delta_{g}$ excited state of O₂. However, previous theoretical investigations have identified a low-lying singlet biradical excited state in analogy to the $^1\Sigma_{\sigma}^+$ excited state of O_2 for [CuO]+ species similar to the ones described here [24], and as such the ability to distinguish between these three cases is necessary to correctly identify the ground state of the [CuO]⁺ species generated from 1 to 3.

Active spaces of 12 electrons in 12 orbitals were first constructed from MOs derived from the Cu 3d orbitals, the O 2p orbitals, and the Cu 4d orbitals (Figs. S7–9). Applying the CASSCF/NEVPT2 method to [1-O] $^+$, an S = 1 ground state is predicted with a low-lying S = 0 excited state separated by 0.215 eV (4.97 kcal mol $^{-1}$) (Table S5). The triplet ground state is well-described by a single configuration, however, the

electronic structure does not rigidly conform to a simple Cu^{II} -oxyl picture as expected. Rather, the MOs occupied by the two radicals are more covalent in nature, complicating the analysis. Similar electronic structures were predicted for $[2\text{-}O]^+$ and $[3\text{-}O]^+$ with an active space of 12 electrons in 12 orbitals (Figs. S8–9, Tables S6-7). The CAS(12,12) results are best described as existing on a continuum between the extremes of a Cu^{II} -oxyl formulation and a Cu^{II} -bound biradicaloid oxene, somewhat to our surprise. This is not, however, an unprecedented result for first-row transition metals and intermediates with similar electronic structures have been proposed as in the case of a biradicaloid Co^{II} -oxene species [78], and even isolated and studied spectroscopically in the case of a similar S=1 Cu^{I} -nitrene intermediate [79].

Without any spectroscopic data on [CuO]⁺ compounds available in the literature to calibrate our understanding of the CAS(12,12)/NEVPT2 results, we further extended our computational investigation to probe the sensitivity of the results to active space composition and computational procedure. Alternative active spaces consisting of 14 electrons in 8 orbitals were constructed from MOs derived from the five Cu 3d orbitals and the three O 2p orbitals. The occupation of the resulting orbitals from this step were inspected and those with an occupation less than 1.98 and greater than 0.02 were used as reference spaces for subsequent Spectroscopy ORiented Configuration Interaction (SORCI) calculations (Figs. S10-12). The sufficiency of the reference space was evaluated by ensuring that the weight of the reference configuration in each CI state was greater than 0.90 (Tables S8-10). In each case, a triplet ground state was predicted below a low-lying open shell singlet state. In the case of [1-O]⁺, a multiconfigurational ground state derived from a what is possibly best described as a Cu^I-oxene (CI coefficient 0.39) configuration and two Cu^{II}-oxyl configurations (CI coefficients 0.37 and 0.15, respectively) (Fig. 5, Table S8). The ground state of [2-O]⁺ was well-described by a single configuration (CI coefficient 0.75) (Table S9) and consistent with the Cu^{II}-oxyl formulation. A multiconfigurational ground state was predicted for [3-O]+, however its primary configuration is well-described as a Cu^{II}-oxyl (CI coefficient 0.63) with some

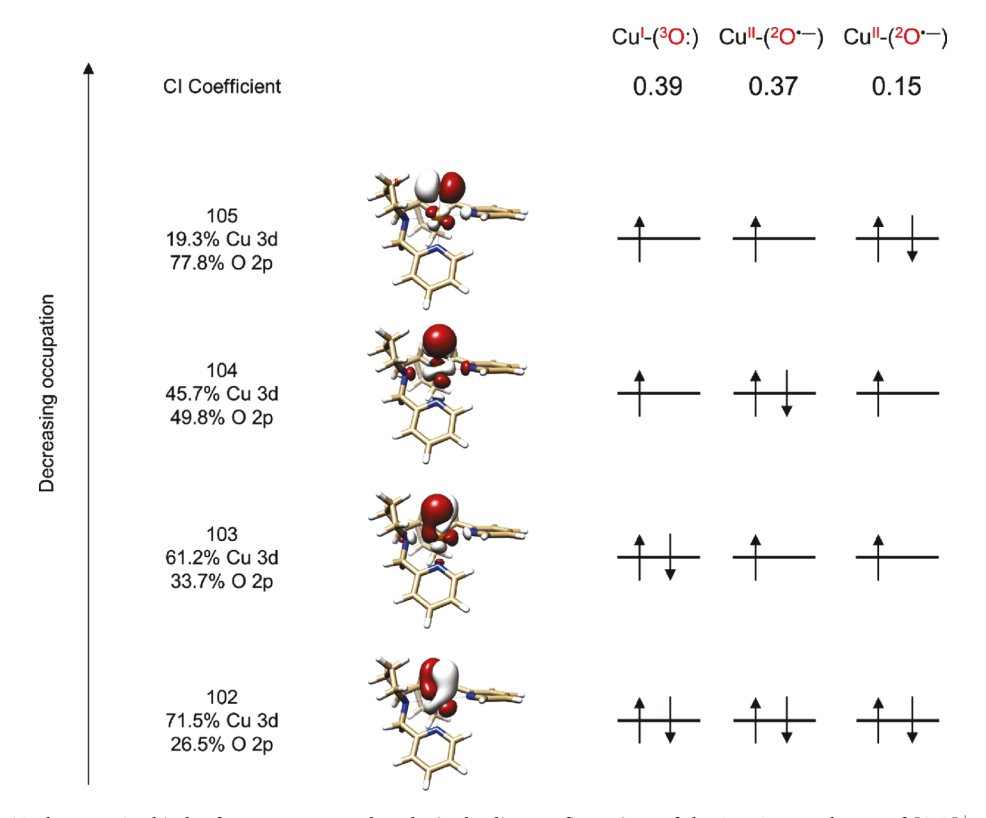


Fig. 5. Subspace of the 10-electron, 6-orbital reference space used to depict leading configurations of the S=1 ground state of $[1-O]^+$ generated from a SORCI calculation. Surface plots of the average atomic natural orbitals are displayed at an isovalue of 0.03 [a.u].

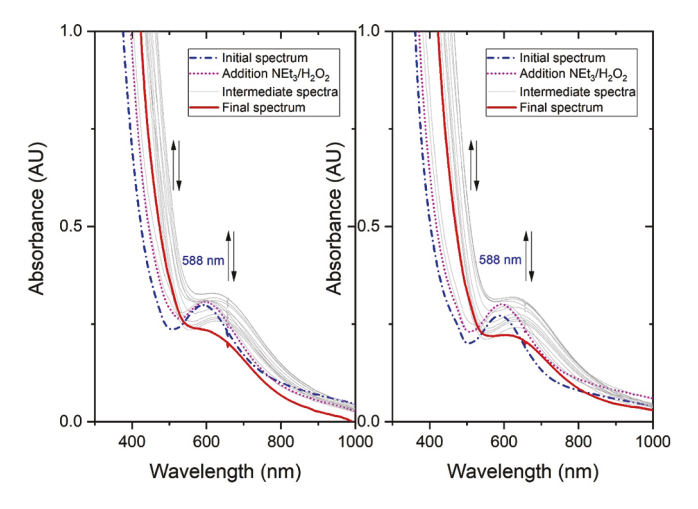


Fig. 6. Left: Reaction of **1** with 10 eq. H_2O_2 , 10 eq. NEt_3 , and 40 eq. styrene in MeCN monitored for 6 h via electronic absorption spectroscopy. Right: Reaction of **1** with 10 eq. H_2O_2 , 10 eq. NEt_3 , and 40 eq. cyclooctene in MeCN monitored for 6 h via electronic absorption spectroscopy. Optical path length 1 cm.

admixture of the Cu^I -oxene configuration (CI coefficient 0.16) (Table S10). The results, though unexpected, were fairly robust to changes in active space and even computational method. Interestingly, we did not identify any state in which the oxidation state could be unambiguously assigned as Cu^{III} .

As both methods predicted either a multiconfigurational or open shell singlet excited state, we calculated the singlet–triplet energy gap (ΔE) for each intermediate within the framework of broken-symmetry (BS) DFT at the B3LYP, M06, and ω B97X levels of theory. All methods conclude that the ground states of $[1\text{-O}]^+$, $[2\text{-O}]^+$, and $[3\text{-O}]^+$ possess spin angular momentum S=1 and the calculated ΔE values are generally of the same order of magnitude (Table 3) except for in the case of $[3\text{-O}]^+$ when ΔE was calculated with the ω B97X functional. However, the amount by which the singlet state was predicted to be lower in energy for $[3\text{-O}]^+$ with the ω B97X functional seems to be within the uncertainty of the functional's general performance [48]. All of the computational methods considered here generally converge to same conclusion: two radicals are localized to the [CuO] core of the ground state of $[1\text{-O}]^+$, $[2\text{-O}]^+$, and $[3\text{-O}]^+$ with spin angular momentum S=1.

The analogous high-valent Fe- and Mn-oxo species are powerful oxidants capable of C—H bond activation and functionalization, but in some cases have also been reported to perform O-atom transfer to olefins to generate epoxides. Cytochrome P450, for example, catalyzes the epoxidation of alkene substrates with an Fe^{IV}-oxo porphyrin cation-radical species [80–83]. Indeed, synthetic iron and manganese porphyrins have been extensively studied for their use as epoxidation catalysts [22,83–87]. However, in some of these reports, the ability to perform epoxidations has been attributed to the oxyl or oxene character – described in different terms over the last few decades - of the active oxidant [80,88,89]. Whether referred to as triplet character, oxenoid character, triplet oxenoid character, or oxyl character, nonzero spin density at the metal-bound oxygen has been cited as necessary for the observed reactivity. If we take this as an assumption, aspects of the calculated electronic structure of the proposed [CuO]⁺ intermediates –

Table 3 Singlet-triplet energy gaps ($\Delta E = E_{triplet} - E_{singlet}$) [eV] for [1-O]⁺, [2-O]⁺, and [3-O]⁺.

| | CAS(12,12)/NEVPT2 | SORCI (10,6) | B3LYP | M06 | ωB97X |
|----------------------------------------------------------------|----------------------------|----------------------------|--------------------------|--------------------------|---------------------------|
| [1-O] ⁺ [2-O] ⁺ [3-O] ⁺ | -0.215 -0.230 -0.219 | -0.134 -0.270 -0.224 | -0.158 -0.158 -0.152 | -0.245 -0.214 -0.239 | -0.163 -0.153 0.033 |

triplet ground state, O-radical character – suggest that [1-O]⁺, [2-O]⁺, and [3-O]⁺ should be capable of performing substrate epoxidation. This is curious as reports of epoxidation catalyzed by mononuclear copper complexes in the literature are extremely rare.

3.5. Olefin epoxidation

To verify that 1-3 could perform O-atom transfer to alkene substrates, we explored their reactivity toward styrene and cyclooctene as we did for CHD and DHA. Treatment of 1 with 10 eq. NEt₃/H₂O₂ in the presence of 40 eq. of styrene or cyclooctene resulted in final absorption spectra (Fig. 6) with increased absorbance in the 400-500 nm region compared to treatment with only NEt₃ and H₂O₂ (Fig. 3). Treatment of 2 with 10 eq. NEt₃/H₂O₂ in the presence of 40 eq. of styrene did not result in noticeable changes to the final absorption spectrum when compared to treatment with only NEt₃/H₂O₂, though this was not the case in the presence of 40 eq. of cyclooctene (Figs. S13-14). Complex 3 behaved similarly to complex 1 (Figs. S15–16). Analysis of the product solutions by GC-MS confirmed the presence of cyclooctene oxide (Table 4). Benzaldehyde, rather than styrene oxide, was observed - but it is important to note that styrene oxide has been reported to be further oxidized to benzaldehyde under similar reaction conditions and thus its initial formation cannot be rejected [90]. Treatment of cyclooctene with NEt₃/H₂O₂ in the presence of copper(II) perchlorate did result in some formation of cyclooctene oxide, but in a lower yield than observed with 1–3, suggesting that the ligand supporting the copper center does play a role in modulating its reactivity.

4. Summary

A detailed investigation of the reactivity of three mononuclear Cu^{II} complexes supported by [N4] polypyridyl ligands using a combined experimental and theoretical approach is presented herein. Consistent with previously reported Cu^{II}-bispicen complexes, 1–3 were capable of C-H bond activation in the presence of NEt₃ and H₂O₂ (Fig. 7). A computational investigation into the electronic structure of the proposed [CuO]⁺ reactive intermediates revealed a complex triplet ground state. Mapping the spatial distribution of the radicals localized to the [CuO] core of the proposed [CuO] $^+$ intermediates onto a single electron configuration proved challenging. The predicted electronic structures were generally consistent with a Cu^{II}-oxyl species, noting the corresponding Cu^I-oxene species as a possibly significant resonance structure. Correlating the electronic structure of the proposed [CuO]⁺ intermediates to those of analogous high-valent metal-oxo species capable of performing substrate epoxidation, we predicted that 1-3, too, should be capable of substrate epoxidation when treated with NEt₃/H₂O₂ and alkenes. Cyclooctene oxide was obtained as the product upon treatment of 1-3 with NEt₃/H₂O₂ in the presence of cyclooctene (Fig. 7). These results represent one of the first reports of epoxidation performed by mononuclear copper complexes, to our knowledge, warranting further investigation into the complex electronic structure and diverse reactivity of high-valent [CuO]+ species.

CRediT authorship contribution statement

Thomas M. Khazanov: Conceptualization, Methodology, Investigation, Formal analysis, Visualization. Niharika Krishna Botcha: Investigation, Formal analysis, Visualization. Sandugash Yergeshbayeva: Investigation, Resources. Michael Shatruk: Investigation, Resources, Supervision, Funding acquisition. Anusree Mukherjee: Conceptualization, Methodology, Supervision, Project administration, Funding acquisition.

Declaration of Competing Interest

The authors declare that they have no known competing financial

Table 4Reaction mixture product analysis.

| Complex | Benzene | Anthraquinone | Anthracene | Anthrone | Benzaldehyde | Styrene Oxide | Cyclooctene Oxide |
|---------------|------------|---------------|------------|-----------|--------------|---------------|-------------------|
| 1 | $47\pm4\%$ | $20\pm0\%$ | $19\pm1\%$ | $3\pm0\%$ | $8\pm1\%$ | 0% | $16\pm2\%$ |
| 2 | $52\pm7\%$ | $21\pm0\%$ | $19\pm0\%$ | $3\pm0\%$ | $10\pm1\%$ | $1\pm0\%$ | $15\pm1\%$ |
| 3 | $52\pm4\%$ | $21\pm1\%$ | $20\pm0\%$ | $4\pm0\%$ | $9\pm1\%$ | 0% | $18\pm1\%$ |
| $Cu(ClO_4)_2$ | 0% | 0% | 0% | 0% | 0% | 0% | $8\pm1\%$ |
| No Cu | $3\pm0\%$ | $2\pm0\%$ | $2\pm0\%$ | 0% | 0% | 0% | $1\pm0\%$ |

Fig. 7. Summary of the proposed reactivity of 1-3.

interests or personal relationships that could have appeared to influence the work reported in this paper.

Acknowledgements

This work was made possible in part by a grant of high-performance computing resources and technical support from the Alabama Supercomputer Authority. T.K. graciously thanks the Lancaster research group at Cornell University for use of computing resources. M.S. and Y.S. acknowledge support by the National Science Foundation (award CHE-1955754). The Rigaku Synergy-S single-crystal X-ray diffractometer used for crystallographic work was acquired through the NSF MRI program (award CHE-1828362 to M.S.). T.K., N.K.B., and A.M. acknowledge support from the University of Alabama in Huntsville for conducting this research work.

Appendix A. Supplementary data

Supplementary data to this article can be found online at https://doi.org/10.1016/j.ica.2020.120168.

References

- [1] E.I. Solomon, D.E. Heppner, E.M. Johnston, J.W. Ginsbach, J. Cirera, M. Qayyum, M.T. Kieber-Emmons, C.H. Kjaergaard, R.G. Hadt, L. Tian, Copper active sites in biology, Chem. Rev. 114 (7) (2014) 3659–3853, https://doi.org/10.1021/cr400327t
- [2] J.J. Liu, D.E. Diaz, D.A. Quist, K.D. Karlin, Copper(I)-dioxygen adducts and copper enzyme mechanisms, Isr. J. Chem. 56 (2016) 9–10, https://doi.org/10.1002/ iich.201600025.
- [3] C.E. Elwell, N.L. Gagnon, B.D. Neisen, D. Dhar, A.D. Spaeth, G.M. Yee, W. B. Tolman, Copper-oxygen complexes revisited: structures, spectroscopy, and reactivity, Chem. Rev. 117 (3) (2017) 2059–2107, https://doi.org/10.1021/acs.chemrev.6b00636.
- [4] C. Citek, S. Herres-Pawlis, T.D.P. Stack, Low temperature syntheses and reactivity of Cu2O2 active-site models, Acc. Chem. Res. 48 (8) (2015) 2424–2433, https://doi.org/10.1021/acs.accounts.5b00220.
- [5] R. Trammell, K. Rajabimoghadam, I. Garcia-Bosch, Copper-promoted functionalization of organic molecules: from biologically relevant Cu/O₂ model systems to organometallic transformations, Chem. Rev. 119 (4) (2019) 2954–3031, https://doi.org/10.1021/acs.chemrev.8b00368.
- [6] E.I. Solomon, P. Chen, M. Metz, S.-K. Lee, A.E. Palmer, Oxygen binding, activation, and reduction to water by copper proteins, Angew. Chem. Int. Ed. 21 (2001).
- [7] J.Y. Lee, K.D. Karlin, Elaboration of copper-oxygen mediated C-H activation chemistry in consideration of future fuel and feedstock generation, Curr. Opin. Chem. Biol. 25 (2015) 184–193.
- [8] M.O. Ross, F. MacMillan, J. Wang, A. Nisthal, T.J. Lawton, B.D. Olafson, S.L. Mayo, A.C. Rosenzweig, B.M. Hoffman, Particulate methane monooxygenase contains only mononuclear copper centers, Science 364 (6440) (2019) 566–570, https://doi.org/10.1126/science.aav/2572.
- [9] S.Y. Ro, L.F. Schachner, C.W. Koo, R. Purohit, J.P. Remis, G.E. Kenney, B.W. Liauw, P.M. Thomas, S.M. Patrie, N.L. Kelleher, A.C. Rosenzweig, Native top-down mass spectrometry provides insights into the copper centers of membrane-bound

- methane monooxygenase, Nat Commun 10 (1) (2019) 2675, https://doi.org/10.1038/s41467-019-10590-6.
- [10] T. Kamachi, N. Kihara, Y. Shiota, K. Yoshizawa, Computational exploration of the catalytic mechanism of dopamine β-monoxygenase: modeling of its mononuclear copper active sites, Inorg. Chem. 44 (12) (2005) 4226–4236, https://doi.org/ 10.1021/jc048477n.
- [11] K. Yoshizawa, N. Kihara, T. Kamachi, Y. Shiota, Catalytic mechanism of dopamine β-monooxygenase mediated by Cu(III)—oxo, Inorg. Chem. 45 (7) (2006) 3034–3041, https://doi.org/10.1021/ic0521168.
- [12] A. Decker, E.I. Solomon, Dioxygen activation by copper, heme and non-heme iron enzymes: comparison of electronic structures and reactivities, Curr. Opin. Chem. Biol. 9 (2) (2005) 152–163, https://doi.org/10.1016/j.cbpa.2005.02.012.
- [13] K. Rudzka, D.M. Moreno, B. Eipper, R. Mains, D.A. Estrin, L.M. Amzel, Coordination of peroxide to the CuM center of peptidylglycine α-hydroxylating monooxygenase (PHM): structural and computational study, J. Biol. Inorg. Chem. 18 (2) (2013) 223–232, https://doi.org/10.1007/s00775-012-0967-z.
- [14] S. Kim, J. Ståhlberg, M. Sandgren, R.S. Paton, G.T. Beckham, Quantum Mechanical Calculations Suggest That Lytic Polysaccharide Monooxygenases Use a Copper-Oxyl, Oxygen-Rebound Mechanism, Proc Natl Acad Sci U S A 111 (1) (2014) 149–154, https://doi.org/10.1073/pnas.1316609111.
- [15] L. Cao, O. Caldararu, A.C. Rosenzweig, U. Ryde, Quantum refinement does not support dinuclear copper sites in crystal structures of particulate methane monooxygenase, Angew. Chem. Int. Ed. 57 (1) (2018) 162–166, https://doi.org/ 10.1002/anie.2017.08977
- [16] K. Yoshizawa, Y. Shiota, Conversion of methane to methanol at the mononuclear and dinuclear copper sites of particulate methane monooxygenase (PMMO): a DFT and QM/MM study, J. Am. Chem. Soc. 128 (30) (2006) 9873–9881, https://doi. org/10.1021/ja061604r.
- [17] S.T. Kleespies, W.N. Oloo, A. Mukherjee, L. Que, C-H bond cleavage by bioinspired nonheme oxoiron(IV) complexes, including hydroxylation of *n*-butane, Inorg. Chem. 54 (11) (2015) 5053–5064, https://doi.org/10.1021/ic502786y.
- [18] A.N. Biswas, M. Puri, K.K. Meier, W.N. Oloo, G.T. Rohde, E.L. Bominaar, E. Münck, L. Que, Modeling TauD-J: a high-spin nonheme oxoiron(IV) complex with high reactivity toward C-H bonds, J. Am. Chem. Soc. 137 (7) (2015) 2428–2431, https://doi.org/10.1021/ja511757j.
- [19] C. Krebs, D. Galonić Fujimori, C.T. Walsh, J.M. Bollinger, Non-Heme Fe(IV)–Oxo intermediates, Acc. Chem. Res. 40 (7) (2007) 484–492, https://doi.org/10.1021/ ar700066p.
- [20] J. Hohenberger, K. Ray, K. Meyer, The biology and chemistry of high-valent iron-oxo and iron-nitrido complexes, Nat Commun 3 (1) (2012) 720, https://doi.org/10.1038/ncomms1718.
- [21] M. Balamurugan, N. Saravanan, H. Ha, Y.H. Lee, K.T. Nam, Involvement of high-valent manganese-oxo intermediates in oxidation reactions: realisation in nature, nano and molecular systems, Nano Convergence 5 (1) (2018) 18, https://doi.org/10.1186/s40580-018-0150-5.
- [22] M. Guo, T. Corona, K. Ray, W. Nam, Heme and nonheme high-valent iron and manganese oxo cores in biological and abiological oxidation reactions, ACS Cent. Sci. 5 (1) (2019) 13–28, https://doi.org/10.1021/acscentsci.8b00698.
- [23] R.L. Halbach, D. Gygi, E.D. Bloch, B.L. Anderson, D.G. Nocera, Structurally characterized terminal manganese(IV) oxo tris(Alkoxide) complex, Chem. Sci. 9 (19) (2018) 4524–4528, https://doi.org/10.1039/C8SC01164H.
- [24] S.M. Huber, M.Z. Ertem, F. Aquilante, L. Gagliardi, W.B. Tolman, C.J. Cramer, Generating CuII–Oxyl/CuIII–Oxo species from CuI–α-ketocarboxylate complexes and O2. In silico studies on ligand effects and C H-activation reactivity, Chem. – A Eur. J. 15 (19) (2009) 4886–4895, https://doi.org/10.1002/chem.200802338.
- [25] N. Singh, N.K. Botcha, T.M. Jones, M.Z. Ertem, J. Niklas, E.R. Farquhar, O. G. Poluektov, A. Mukherjee, Reactivity of bio-inspired Cu(II) (N2/Py2) complexes with peroxide at room temperature, J. Inorg. Biochem. 197 (2019), 110674, https://doi.org/10.1016/j.jinorgbio.2019.03.014.
- [26] A.W. Munro, K.J. McLean, J.L. Grant, T.M. Makris, Structure and function of the cytochrome P450 peroxygenase enzymes, Biochem. Soc. Trans. 46 (1) (2018) 183–196, https://doi.org/10.1042/BST20170218.
- [27] J.P.T. Zaragoza, T.H. Yosca, M.A. Siegler, P. Moënne-Loccoz, M.T. Green, D. P. Goldberg, Direct observation of oxygen rebound with an iron-hydroxide complex, J. Am. Chem. Soc. 139 (39) (2017) 13640–13643, https://doi.org/10.1021/jacs.7b07979.
- [28] B.J. Pella, J. Niklas, O.G. Poluektov, A. Mukherjee, Effects of denticity and ligand rigidity on reactivity of copper complexes with cumyl hydroperoxide, Inorg. Chim. Acta 483 (2018) 71–78, https://doi.org/10.1016/j.ica.2018.07.035.
- [29] P.H.A. Kankanamalage, D.M. Ekanayake, N. Singh, A.C.P. Morais, S. de Mazumder, C.N. Verani, A. Mukherjee, M. Lanznaster, Effect of ligand substituents on nickel and copper [N4] complexes: electronic and redox behavior, and reactivity towards protons, New J. Chem. 43 (32) (2019) 12795–12803, https://doi.org/10.1039/ C9NJ01283D.

- [30] Software update: the ORCA program system, version 4.0 Neese 2018 WIREs Computational Molecular Science – Wiley Online Library https://onlinelibrary. wiley.com/doi/abs/10.1002/wcms.1327 (accessed Jan 10, 2020).
- [31] A.D. Becke, Completely numerical calculations on diatomic molecules in the local-density approximation, Phys. Rev. A 33 (4) (1986) 2786–2788, https://doi.org/10.1103/PhysRevA.33.2786.
- [32] J.P. Perdew, Density-functional approximation for the correlation energy of the inhomogeneous electron gas, Phys. Rev. B 33 (12) (1986) 8822–8824, https://doi. org/10.1103/PhysRevB.33.8822.
- [33] F. Weigend, R. Ahlrichs, Balanced basis sets of split valence, triple zeta valence and quadruple zeta valence quality for H to Rn: design and assessment of accuracy, Phys. Chem. Chem. Phys. 7 (18) (2005) 3297–3305, https://doi.org/10.1039/ B508541A.
- [34] A. Schäfer, C. Huber, R. Ahlrichs, Fully optimized contracted gaussian basis sets of triple zeta valence quality for atoms Li to Kr, J. Chem. Phys. 100 (8) (1994) 5829–5835, https://doi.org/10.1063/1.467146.
- [35] A. Schäfer, H. Horn, R. Ahlrichs, Fully optimized contracted gaussian basis sets for atoms Li to Kr, J. Chem. Phys. 97 (4) (1992) 2571–2577, https://doi.org/10.1063/ 1.462006
- [36] S. Grimme, S. Ehrlich, L. Goerigk, Effect of the damping function in dispersion corrected density functional theory, J. Comput. Chem. 32 (7) (2011) 1456–1465, https://doi.org/10.1002/jcc.21759.
- [37] S. Grimme, J. Antony, S. Ehrlich, H. Krieg, A consistent and accurate ab initio parametrization of density functional dispersion correction (DFT-D) for the 94 elements H-Pu, J. Chem. Phys. 132 (15) (2010), 154104, https://doi.org/10.1063/ 1.338/344
- [38] F. Neese, F. Wennmohs, A. Hansen, Becker U. Efficient, Approximate and parallel hartree-fock and hybrid DFT calculations. A 'chain-of-spheres' algorithm for the hartree-fock exchange, Chem. Phys. 356 (1) (2009) 98–109, https://doi.org/ 10.1016/j.chemphys.2008.10.036.
- [39] F. Weigend, Accurate coulomb-fitting basis sets for H to Rn, Phys. Chem. Chem. Phys. 8 (9) (2006) 1057–1065, https://doi.org/10.1039/b515623h.
- [40] A.D. Becke, Density-functional thermochemistry. III. The role of exact exchange, J. Chem. Phys. 98 (7) (1993) 5648–5652, https://doi.org/10.1063/1.464913.
- [41] C. Lee, W. Yang, R.G. Parr, Development of the Colle-Salvetti correlation-energy formula into a functional of the electron density, Phys. Rev. B 37 (2) (1988) 785–789, https://doi.org/10.1103/PhysRevB.37.785.
- [42] E. Lenthe, E.J. van Baerends, J.G. Snijders, Relativistic regular two-component hamiltonians, J. Chem. Phys. 99 (6) (1993) 4597–4610, https://doi.org/10.1063/ 1.466059.
- [43] E. van Lenthe, E.J. Baerends, J.G. Snijders, Relativistic total energy using regular approximations, J. Chem. Phys. 101 (11) (1994) 9783–9792, https://doi.org/ 10.1063/1.467043
- [44] C. van Wüllen, Molecular density functional calculations in the regular relativistic approximation: method, application to coinage metal diatomics, hydrides, fluorides and chlorides, and comparison with first-order relativistic calculations, J. Chem. Phys. 109 (2) (1998) 392–399, https://doi.org/10.1063/1.476576.
- [45] G.L. Stoychev, A.A. Auer, F. Neese, Automatic generation of auxiliary basis sets, J. Chem. Theory Comput. 13 (2) (2017) 554–562, https://doi.org/10.1021/acs. jctc.6b01041.
- [46] S. Grimme, A simplified Tamm-Dancoff density functional approach for the electronic excitation spectra of very large molecules, J. Chem. Phys. 138 (24) (2013), 244104, https://doi.org/10.1063/1.4811331.
- [47] Y. Zhao, D.G. Truhlar, The M06 suite of density functionals for main group thermochemistry, thermochemical kinetics, noncovalent interactions, excited states, and transition elements: two new functionals and systematic testing of four M06-class functionals and 12 other functionals, Theor. Chem. Account 120 (1) (2008) 215-241, https://doi.org/10.1007/s00214-007-0310-x.
- [48] J.-D. Chai, M. Head-Gordon, Systematic optimization of long-range corrected hybrid density functionals, J. Chem. Phys. 128 (8) (2008), 084106, https://doi. org/10.1063/1.2834918
- [49] B.O. Roos, P.R. Taylor, P.E.M. Sigbahn, A complete active space SCF method (CASSCF) using a density matrix formulated super-CI approach, Chem. Phys. 48 (2) (1980) 157–173, https://doi.org/10.1016/0301-0104(80)80045-0.
- [50] C. Angeli, R. Cimiraglia, S. Evangelisti, T. Leininger, J.-P. Malrieu, Introduction of N-electron valence states for multireference perturbation theory, J. Chem. Phys. 114 (23) (2001) 10252–10264, https://doi.org/10.1063/1.1361246.
- [51] C. Angeli, R. Cimiraglia, J.-P. Malrieu, N-electron valence state perturbation theory: a spinless formulation and an efficient implementation of the strongly contracted and of the partially contracted variants, J. Chem. Phys. 117 (20) (2002) 9138–9153, https://doi.org/10.1063/1.1515317.
- [52] F. Neese, A spectroscopy oriented configuration interaction procedure, J. Chem. Phys. 119 (18) (2003) 9428–9443, https://doi.org/10.1063/1.1615956.
- [53] CrysAlis, Oxford Diffraction Ltd., Abingdon, England, 2006.
- [54] SCALE3 ABSPACK An Oxford Diffraction Program (1.0.4,Gui:1.0.3), Oxford Diffraction Ltd., Abingdon, England, 2005.
- [55] G.M. Sheldrick, Crystal structure refinement with SHELXL, Acta Crystallogr. C Struct. Chem. 71 (1) (2015) 3–8, https://doi.org/10.1107/S2053229614024218.
- [56] O.V. Dolomanov, L.J. Bourhis, R.J. Gildea, J.A.K. Howard, H. Puschmann, OLEX2: a complete structure solution, refinement and analysis program, J. Appl. Crystallogr. 42 (2) (2009) 339–341, https://doi.org/10.1107/ S0021889808042726.
- [57] M.S. Chen, M.C. White, A predictably selective aliphatic C-H oxidation reaction for complex molecule synthesis, Science 318 (5851) (2007) 783–787, https://doi.org/ 10.1126/science.1148597.

- [58] S.L. Esarey, J.C. Holland, B.M. Bartlett, Determining the fate of a non-heme iron oxidation catalyst under illumination, oxygen, and acid, Inorg. Chem. 55 (21) (2016) 11040–11049, https://doi.org/10.1021/acs.inorgchem.6b01538.
- [59] S.J. Brudenell, L. Spiccia, E.R.T. Tiekink, Binuclear copper(II) complexes of bis (pentadentate) ligands derived from alkyl-bridged Bis(1,4,7-Triazacyclonane) macrocycles, Inorg. Chem. 35 (7) (1996) 1974–1979, https://doi.org/10.1021/ ico51146f
- [60] S.S. Massoud, F.R. Louka, R.N. David, M.J. Dartez, Q.L. Nguyn, N.J. Labry, R. C. Fischer, F.A. Mautner, Five-coordinate metal(II) complexes based pyrazolyl ligands, Polyhedron 90 (2015) 258–265, https://doi.org/10.1016/j.poly.2015.02.014
- [61] S.S. Massoud, F.R. Louka, L.T. Nguyen, M. Mikuriya, J.H. Albering, F.A. Mautner, Structural and magnetic characterization of 1-D complexes constructed from pyrazole-3,5-dicarboxylate bridging multi copper(II) centers, Inorg. Chim. Acta 366 (1) (2011) 394–398, https://doi.org/10.1016/j.ica.2010.11.014.
- [62] G.A. McLachlan, G.D. Fallon, R.L. Martin, L. Spiccia, Synthesis, structure and properties of five-coordinate copper(II) complexes of pentadentate ligands with pyridyl pendant arms, Inorg. Chem. 34 (1) (1995) 254–261, https://doi.org/ 10.1021/ic00105a041.
- [63] N. Singh, J. Niklas, O. Poluektov, K.M. Van Heuvelen, A. Mukherjee, Mononuclear nickel (II) and copper (II) coordination complexes supported by bispicen ligand derivatives: experimental and computational studies, Inorg. Chim. Acta 455 (2017) 221–230, https://doi.org/10.1016/j.ica.2016.09.001.
- [64] J.N. Harvey, On the accuracy of density functional theory in transition metal chemistry, Annu. Rep. Prog. Chem., Sect. C: Phys. Chem. 102 (2006) 203, https:// doi.org/10.1039/b419105f.
- [65] R.R. Jacobson, Zoltan Tyeklar, K.D. Karlin, Jon Zubieta, Fluoride as a terminal and bridging ligand for copper: isolation and x-ray crystallographic characterization of copper monomeric and dimeric complexes [CuII(TMPA)F]Nn+ (n = 1 or 2; TMPA = Tris[(2-Pyridyl)Methyl]Amine), Inorg. Chem. 30 (9) (1991) 2035–2040, https://doi.org/10.1021/ic00009a017.
- [66] B.J. Hathaway, The correlation of the electronic properties and stereochemistry of mononuclear CuN 4–6 chromophores, J. Chem. Soc., Dalton Trans. 12 (1972) 1196–1199, https://doi.org/10.1039/DT9720001196.
- [67] A. Kaur, T.G. Ribelli, K. Schröder, K. Matyjaszewski, T. Pintauer, Properties and ATRP activity of copper complexes with substituted Tris(2-Pyridylmethyl)aminebased ligands, Inorg. Chem. 54 (4) (2015) 1474–1486, https://doi.org/10.1021/ ic502484.
- [68] N. Hall, M. Orio, M. Gennari, C. Wills, F. Molton, C. Philouze, G.B. Jameson, M. A. Halcrow, A.G. Blackman, C. Duboc, Multifrequency Cw-EPR and DFT studies of an apparent compressed octahedral Cu(II) complex, Inorg. Chem. 55 (4) (2016) 1497–1504, https://doi.org/10.1021/acs.inorgchem.5b02287.
- [69] E. Garribba, G. Micera, The determination of the geometry of Cu(II) complexes: an EPR spectroscopy experiment, J. Chem. Educ. 83 (8) (2006) 1229, https://doi.org/ 10.1021/ed08301229.
- [70] A. Kunishita, M. Kubo, H. Ishimaru, T. Ogura, H. Sugimoto, S. Itoh, H2O2-reactivity of copper(II) complexes supported by Tris[(Pyridin-2-YI)Methyl]amine ligands with 6-phenyl substituents, Inorg. Chem. 47 (24) (2008) 12032–12039, https://doi.org/10.1021/ic801568g.
- [71] S. Ye, G. Xue, I. Krivokapic, T. Petrenko, E. Bill, L. Que Jr, F. Neese, Magnetic circular dichroism and computational study of mononuclear and dinuclear iron(IV) Complexes, Chem. Sci. 6 (5) (2015) 2909–2921, https://doi.org/10.1039/ C45C03368C
- [72] Christopher J Kramer. Essentials of Computational Chemistry: Theories and Models, Second Edition.; John Wiley & Sons.
- [73] Moffitt, W. The Electronic Structure of the Oxygen Molecule. Proceedings of the Royal Society of London. Series A, Containing Papers of a Mathematical and Physical Character 1951, 210, 224–245.
- [74] W. Orellana, A. da Silva, A. Fazzio, O2 diffusion in SiO2: triplet versus singlet, Phys. Rev. Lett. 87 (15) (2001), 155901, https://doi.org/10.1103/ PhysRevLett.87.155901.
- [75] F. Neese, M. Atanasov, G. Bistoni, D. Maganas, S. Ye, Chemistry and quantum mechanics in 2019: give us insight and numbers, J. Am. Chem. Soc. 141 (7) (2019) 2814–2824, https://doi.org/10.1021/jacs.8b13313.
- [76] S. Jockusch, N.J. Turro, E.K. Thompson, M. Gouterman, J.B. Callis, G.E. Khalil, Singlet molecular oxygen by direct excitation, Photochem. Photobiol. Sci. 7 (2) (2008) 235–239, https://doi.org/10.1039/B714286B.
- [77] C. Schweitzer, R. Schmidt, Physical mechanisms of generation and deactivation of singlet oxygen, Chem. Rev. 103 (5) (2003) 1685–1758, https://doi.org/10.1021/ crol.0321d
- [78] D.W. Crandell, S. Ghosh, C.P. Berlinguette, M.H. Baik, How a [Co IV \${^ {\underline{.....}}}\$0] 2+ Fragment Oxidizes Water: Involvement of a Biradicaloid [Co II -(·O·)] 2+ Species in Forming the O O Bond. ChemSusChem 2015, 8 (5), 844–852. https://doi.org/10.1002/cssc.201403024.
- [79] K.M. Carsch, I.M. DiMucci, D.A. Iovan, A. Li, S.-L. Zheng, C.J. Titus, S.J. Lee, K. D. Irwin, D. Nordlund, K.M. Lancaster, T.A. Betley, Synthesis of a copper-supported triplet nitrene complex pertinent to copper-catalyzed amination, Science 365 (6458) (2019) 1138–1143, https://doi.org/10.1126/science.aax4423.
- [80] D. Ostovic, T.C. Bruice, Mechanism of alkene epoxidation by iron, chromium, and manganese higher valent oxo-metalloporphyrins, Acc. Chem. Res. 25 (7) (1992) 314–320, https://doi.org/10.1021/ar00019a007.
- [81] J. Rittle, M.T. Green, Cytochrome P450 compound I: capture, characterization, and C-H bond activation kinetics, Science 330 (6006) (2010) 933–937, https://doi.org/ 10.1126/science.1193478
- [82] D. Kumar, B. Karamzadeh, G.N. Sastry, S.P. de Visser, What factors influence the rate constant of substrate epoxidation by compound I of cytochrome P450 and

- analogous iron(IV)-oxo oxidants? J. Am. Chem. Soc. 132 (22) (2010) 7656–7667, https://doi.org/10.1021/ja9106176.
- [83] J.T. Groves, M.K. Stern, Synthesis, characterization, and reactivity of oxomanganese(IV) porphyrin complexes, J. Am. Chem. Soc. 110 (26) (1988) 8628–8638, https://doi.org/10.1021/ja00234a009.
- [84] R.D. Arasasingham, G.X. He, T.C. Bruice, Mechanism of manganese porphyrincatalyzed oxidation of alkenes. Role of manganese(IV)-Oxo species, J. Am. Chem. Soc. 115 (18) (1993) 7985–7991, https://doi.org/10.1021/ja00071a008.
- [85] J.T. Groves, M.K. Stern, Olefin epoxidation by manganese (IV) porphyrins: evidence for two reaction pathways, J. Am. Chem. Soc. 109 (12) (1987) 3812–3814, https://doi.org/10.1021/ja00246a067.
- [86] J.T. Groves, Yoshihito Watanabe, The Mechanism of Olefin Epoxidation by Oxo-Iron Porphyrins. Direct Observation of an Intermediate, J. Am. Chem. Soc. 108 (3) (1986) 507–508, https://doi.org/10.1021/ja00263a026.
- [87] R.W. Lee, P.C. Nakagaki, P.N. Balasubramanian, T.C. Bruice, Observations and comments on the mechanism of epoxidation of alkenes by manganese(III)

- porphyrins with hypochlorite, Proc. Natl. Acad. Sci. 85 (3) (1988) 641–644, https://doi.org/10.1073/pnas.85.3.641.
- [88] D. Ricciarelli, Q.M. Phung, L. Belpassi, J.N. Harvey, P. Belanzoni, Understanding the reactivity of Mn-oxo porphyrins for substrate hydroxylation: theoretical predictions and experimental evidence reconciled, Inorg. Chem. 58 (11) (2019) 7345–7356, https://doi.org/10.1021/acs.inorgchem.9b00476.
- [89] G.H. Loew, C.J. Kert, L.M. Hjelmeland, R.F. Kirchner, Active site models of horseradish peroxidase compound I and a cytochrome P-450 analog: electronic structure and electric field gradients, J. Am. Chem. Soc. 99 (10) (1977) 3534–3536, https://doi.org/10.1021/ja00452a074.
- [90] T.A.G. Duarte, A.C. Estrada, M.M.Q. Simões, I.C.M.S. Santos, A.M.V. Cavaleiro, M. G.P.M.S. Neves, J.A.S. Cavaleiro, Homogeneous catalytic oxidation of styrene and styrene derivatives with hydrogen peroxide in the presence of transition metal-substituted polyoxotungstates, Catal. Sci. Technol. 5 (1) (2015) 351–363, https://doi.org/10.1039/C4CY00702P.